

Probing IC/CMB Interpretation for the X-ray knots of AGN through VHE observations

Amal A. Rahman^{1*}, S. Sahayanathan^{2,3†}, Malik Zahoor⁴ and P. A Subha¹

¹*Department of Physics, Farook College, Calicut University, Kerala-673632, India*

²*Astrophysical Sciences Division, Bhabha Atomic Research Centre, Mumbai - 400085, India*

³*Homi Bhabha National Institute, Mumbai 400094, India*

⁴*Department of Physics, University of Kashmir, Srinagar 190006, India*

Accepted XXX. Received YYY; in original form ZZZ

ABSTRACT

Detection of hard X-ray spectrum (spectral index < 2) from the kilo-parsec scale jet of active galactic nuclei cannot be accounted to the synchrotron emission mechanism from the electron distribution responsible for the radio/optical emission. Alternate explanations are the inverse Compton scattering of cosmic microwave background photons (IC/CMB) or synchrotron emission from a second electron population. When the X-ray emission is interpreted as IC/CMB process, the Compton spectrum often peaks at GeV energy and many sources were predicted to be the Fermi candidate sources. The absence of significant gamma ray flux from some of these galaxies by Fermi disfavored the IC/CMB interpretation of the high energy emission. We extend this study to predict the very high energy (VHE) gamma ray emission due to IC/CMB model which can be investigated by Cherenkov Telescope Array Observatory (CTAO). The model parameters deciding the broadband spectral energy distribution are estimated using analytical approximation of the emissivity functions. The emission model is extrapolated to VHE energy and then compared with the CTAO sensitivity. For this particular study, we have selected 18 knots with harder X-ray spectrum and for which the IC/CMB model for X-ray emission was suggested.

Key words: galaxies: active – galaxies: individual: 3C 111; 3C 120 – galaxies: jets – gamma-rays: galaxies – radiation mechanisms: non-thermal

1 INTRODUCTION

Localized brightness enhancements found in the kpc/Mpc scale jets of active galactic nuclei (AGN) are commonly termed as knots (Harris & Krawczynski 2006). These knots are well resolved in radio and optical wavebands. With the advent of high spatial resolution *Chandra* Telescope, the knots were resolved in X-ray bands too. This multi-wavelength emission from AGN knots are generally modeled using synchrotron and inverse Compton emission mechanisms. The radio-to-optical emission is well established as synchrotron emission from a relativistic electron distribution losing its energy in the jet magnetic field. On the other hand, the X-ray emission process is either modelled as the high energy tail of synchrotron spectrum (Hardcastle et al. 2001; Sambruna et al. 2002; Sahayanathan 2008) or as inverse Compton scattering of soft photon field (Tavecchio et al. 2000; Schwartz et al. 2000; Sahayanathan et al. 2003; Perlman et al. 2011).

The high energy emission from knots, when interpreted

as the inverse Compton mechanism, the target photon field at these length scales can be either synchrotron photons (Schwartz et al. 2000); usually called as synchrotron self Compton(SSC) or the ambient cosmic microwave background radiation (Tavecchio et al. 2000; Sambruna et al. 2001); termed IC/CMB mechanism. The SSC interpretation is disfavored as it demands a magnetic field that largely deviates from equipartition (Tavecchio et al. 2000; Harris & Krawczynski 2006). The IC/CMB model; however, requires the jets to be relativistic even at kpc scales so that in the knot frame, the ambient photon field is relativistically boosted to overpower the synchrotron photon energy density. Nevertheless, this interpretation is capable of reproducing the observed X-ray flux from the knots and satisfies near equipartition magnetic field (Sahayanathan et al. 2003; Schwartz et al. 2000; Tavecchio et al. 2000).

The X-ray flux from the knots, when interpreted as IC/CMB process, the Compton spectrum peaks at GeV energy with significant radiation at gamma-ray energies. Hence, *Fermi* observations play a crucial role to validate this emission scenario (Georganopoulos et al. 2006). However, even with a decade of observations, *Fermi*

* E-mail: amalar.amal@gmail.com

† E-mail:sunder@barc.gov.in

failed to detect any appreciable γ -ray photons from some sources and the upper limits drawn fall significantly below the flux predicted by the IC/CMB emission model (Meyer & Georganopoulos 2014; Meyer et al. 2015). Particularly, the γ -ray studies of the *Chandra* detected sources namely, 3C 273(CDQ), PKS 0637-752(CDQ), PKS 1136-135(LDQ), PKS 1229-021(CDQ), PKS 1354+195(CDQ) and PKS 2209+080(CDQ) (Meyer & Georganopoulos 2014; Meyer et al. 2015; Breiding et al. 2017) have strongly ruled out the IC/CMB interpretation but favour a scenario where synchrotron emission from a second population of relativistic electrons being responsible for the observed X-ray emission (Liu et al. 2015; Tavecchio 2021; Harris & Krawczynski 2002; Atoyan & Dermer 2004; Kataoka & Stawarz 2005). In our recent work, we show that the advection of electrons from the regions of particle acceleration can naturally produce two distinct populations which can successfully explain the X-ray emission from the kpc scale knots of 3C 273 (Rahman et al. 2022).

Though recent observational evidence, including γ -ray upper limits, disfavour the IC/CMB interpretation of X-ray emission (Breiding 2018), it is still a preferred model for those sources which are not yet ruled out by *Fermi* observations (Kharb et al. 2012; Godfrey et al. 2012; Stanley et al. 2015). Zhang et al. (2010) present the analysis of 22 hotspots and 45 knots to conclude that IC/CMB model can explain the X-ray emission from the majority of the jet components.

This study was then extended to a larger number of jet components and the jet power is estimated under IC/CMB and SSC emission scenarios for the observed X-ray fluxes (Zhang et al. 2018). The jet power estimated considering IC/CMB strongly correlate with the jet kinetic power obtained through radio studies. Whereas, the SSC interpretation did not exhibit any significant correlation. These findings further supported the

IC/CMB as a promising mechanism to explain the high energy emission from the knots.

Lucchini et al. (2017) revisited some aspects of the IC/CMB model to show the role of electron cooling in shaping the spectrum. They suggest, the overproduction of gamma-rays can be avoided by suppressing the high energy end of the emitting particle population. They applied this model for the case of PKS 0637-752 and demonstrated that IC/CMB can still be a valid explanation for the high energy production from the large scale knots of AGN. In this context, it will be useful to explore the alternative techniques which can supplement the *Fermi* studies to test the plausibility of the IC/CMB interpretation for the high energy emission.

Modelling the X-ray emission from kilo-parsec scale jets using IC/CMB model also suggests this spectrum can extend up to very high energies (VHE) (Meyer et al. 2021, 2019; Georganopoulos et al. 2006). Hence, future VHE observation of these sources can provide further constraints in addition to the ones drawn through *Fermi* observations. The operational ground-based VHE telescopes employing imaging atmospheric Cherenkov techniques have already detected six radio galaxies with mis-aligned jets at GeV/TeV energies (Aleksić et al. 2012; Aharonian et al. 2009, 2006; Holder 2011; Dyrda et al. 2015; Aleksić et al. 2010; Rulten 2022). Among these sources four belong to FRI class of radio galaxies (M87, Cen A, NGC 1275, and 3C 264) while other two (PKS 0625-35 and IC 310) show the properties of radio galaxy

and blazar as well (Wakely & Horan 2008). If IC/CMB is a viable emission process for the X-ray knots, then this suggests many misaligned jets may be a potential TeV candidate. Alternatively, VHE studies can also be a tool to validate this emission scenario in tandem with the *Fermi* observations.

Considerable advancement in the stereoscopic imaging atmospheric Cherenkov techniques have led to new generation VHE telescopes whose sensitivity are appreciable even at few tens of GeV. Particularly, with the inputs from the upcoming Cherenkov Telescope Array (CTA), it may be possible to verify the IC/CMB interpretation of the X-ray knots which were not been ruled out through *Fermi* observations. In the present work, we selected all the kilo parsec scale X-ray jets for which IC/CMB emission process is favoured. We model the radio and optical fluxes from these sources as synchrotron emission from a broken power-law electron distribution. The source parameters are constrained considering equipartition between the magnetic field and the particle energy density. The IC/CMB spectrum is then extrapolated to VHE energies and compared with the CTA sensitivity curves. The paper is organised as follows: In section 2, we describe the source selection and in section 3, the spectral models used in the paper. In section 4 we present our results and discussion. Throughout this work we consider a cosmology where $H_0 = 71 \text{ km s}^{-1} \text{ Mpc}^{-1}$, $\Omega_m = 0.27$ and $\Omega_\Lambda = 0.73$.

2 SOURCE SELECTION

Chandra during its two decades operation was able to resolve nearly 150 X-ray extended features from AGN¹. Many of these extended jet features showed bright knots and hotspots which are coincident (near-coincident) with radio/optical maxima. Spectral energy distribution (SED) of these knots (and unresolved jet features) in radio, optical and X-ray have been already analysed and reported in earlier works (Schwartz et al. 2006; Siemiginowska et al. 2007; Wilson et al. 2001; Chartas et al. 2000). Due to less number of counts, spectral resolution at these energies cannot be achieved and the fluxes were reported only for one or few energy bins (Massaro et al. 2011, 2018; Stuardi et al. 2018). However, convoluting the X-ray instrumental response with a power-law source spectrum, constraints on the spectral index can be obtained and this can be helpful in identifying the emission process.

Among the sample of extended X-ray jets collected from the literature, we selected 18 X-ray knots/components with radio-optical-X-ray observations and a harder X-ray spectrum (spectral index less than 2 or the X-ray flux value larger than high-energy extension of the radio-to-optical synchrotron spectrum). The X-ray emission from these knots were interpreted as IC/CMB. Additionally, for these sources, IC/CMB model were not ruled out by *Fermi* studies until 2023. In Table 1 we provide the list of complete sources and knots.

¹ Xjet:https://hea-www.harvard.edu/XJET/

Source	Type	Knot	z^a	$\text{Log}(F_{\text{obs}}^{\text{r}})^b$	$\text{Log}(F_{\text{obs}}^{\text{o}})^c$	$\text{Log}(F_{\text{obs}}^{\text{x}})^d$	Reference
3C 15	FRI	K C	0.073	-24.63	-28.85	$-31.87^{+0.119}_{-0.108}$	(Dulwich et al. 2007; Kataoka et al. 2003)
3C 17	hybrid	S 3.7	0.22	-24.51	-28.66	$-32.19^{+0.256}_{-0.168}$	Massaro et al. (2009)
3C 17	hybrid	S 11.3	0.22	$-24.10^{+0.04}_{-0.04}$	$-29.64^{+0.07}_{-0.07}$	$-32.27^{+0.15}_{-0.15}$	Massaro et al. (2009)
3C 111	FRII	K 22	0.049	$-25.42^{+0.05}_{-0.06}$	$-29.38^{+0.19}_{-0.18}$	$-32.40^{+0.12}_{-0.12}$	Clautice et al. (2016)
3C 111	FRII	K 30	0.049	-24.86	-28.04	-31.13	Clautice et al. (2016)
3C 111	FRII	K 61	0.049	-24.43	$-28.78^{+0.12}_{-0.11}$	-31.38	Clautice et al. (2016)
3C 120	FRI	K 4	0.033	-24.45	-28.73	$-31.52^{+0.06}_{-0.06}$	Harris et al. (2004)
3C 120	FRI	S 2	0.033	$-24.88^{+0.05}_{-0.05}$	$-28.62^{+0.06}_{-0.06}$	$-32.54^{+0.17}_{-0.17}$	Harris et al. (2004)
PKS 1354+195	CDQ	S 4.0	0.720	-24.96	$-30.07^{+0.09}_{-0.09}$	$-32.27^{+0.06}_{-0.06}$	Harris et al. (2017)
PKS 1354+195	CDQ	S 5.3	0.720	$-25.54^{+0.04}_{-0.04}$	$-30.23^{+0.09}_{-0.09}$	$-32.78^{+0.11}_{-0.11}$	Harris et al. (2017)
3C 346	FRI	K C	0.161	-24.16	$-28.40^{+0.13}_{-0.10}$	$-31.81^{+0.05}_{-0.06}$	Worrall & Birkinshaw (2005)
3C 454.3	CDQ	K A	0.859	-24.39	$-29.92^{+0.09}_{-0.10}$	$-31.24^{+0.08}_{-0.11}$	Tavecchio et al. (2007)
3C 454.3	CDQ	K B	0.859	$-23.71^{+0.04}_{-0.04}$	$-29.31^{+0.03}_{-0.03}$	$-31.25^{+0.11}_{-0.10}$	Tavecchio et al. (2007)
PKS 2101-490	CDQ	K 6	1.040	$-25.12^{+0.02}_{-0.02}$	-29.89	$-32.^{+0.11}_{-0.11}$	Godfrey et al. (2012)
PKS B0106+013	CDQ	K 1	2.11	-24.86	-30.50	-33.08	Kharrb et al. (2012)
PKS B0106+013	CDQ	K 2	2.11	-24.62	-30.41	-33.37	Kharrb et al. (2012)
PKS B0106+013	CDQ	K 3	2.11	-23.74	-30.62	-33.53	Kharrb et al. (2012)
PKS 1045-188	CDQ	K C	0.590	$-24.62^{+0.09}_{-0.09}$	$-30.09^{+0.05}_{-0.05}$	-32.11	Stanley et al. (2015)

Table 1. List of AGNs with Jet Knots/components included in our source list. Notes: a^z , redshift; b^c (col V), c (col VI), d (col VII) are the average observed fluxes in radio, optical and X-ray energies respectively. The energy range over which this fluxes are averaged is mentioned in references (col VIII).

3 IC/CMB MODEL

The radio/optical/X-ray knot buried in AGN jet is considered to be an spherical region of size R_{knot} governed by its radio contour. We assume this region is uniformly populated with a broken power-law electron distribution of the form given by

$$N(\gamma)d\gamma = \begin{cases} K\gamma^{-p}d\gamma & \gamma_{\min} < \gamma < \gamma_b \\ K\gamma_b^{q-p}\gamma^{-q}d\gamma & \gamma_b < \gamma < \gamma_{\max} \end{cases} \quad (1)$$

where, K is the normalisation, γ is the Lorentz factor of the electron and γ_b is the radiative cooling break. The electrons lose their energy through synchrotron and inverse Compton radiative processes. If we consider $P_{\text{rad}}(\gamma, \nu)$ as the single particle emissivity due to these radiative processes, then the total emissivity from the knot can be obtained as (Rybicki & Lightman 1986)

$$J_{\text{rad}}(\nu) = \frac{1}{4\pi} \int_{\gamma_{\min}}^{\gamma_{\max}} P_{\text{rad}}(\gamma, \nu) N(\gamma) d\gamma \quad (2)$$

Here, P_{rad} additionally depend on the magnetic field in case of synchrotron (rad \rightarrow syn) while in case of inverse Compton process, it depends on the target photon energy and distribution (rad \rightarrow ic).

We assume a tangled magnetic field configuration which is in equipartition with the electron distribution (condition that indicates total energy of the system is minimum (Burbidge 1959));

$$\frac{B^2}{8\pi} = m_e c^2 \int_{\gamma_{\min}}^{\gamma_{\max}} N(\gamma) \gamma d\gamma \quad (3)$$

Under delta function approximation for single particle emissivity, an approximate emissivity for synchrotron emission can be obtained as (Dermer & Menon 2009; Sahayanathan & Godambe 2012)

$$J_{\text{syn}}(\nu) \approx \frac{c\sigma_T B^2}{48\pi^2} \nu_L^{-\frac{3}{2}} N \left(\sqrt{\frac{\nu}{\nu_L}} \right) \nu^{\frac{1}{2}} \quad (4)$$

Since the X-ray emission is interpreted as IC/CMB process, we can arrive an analytical form of the IC emissivity by considering the CMB distribution as a monochromatic photon field and a delta function approximation for the P_{ic} (Dermer & Menon 2009; Sahayanathan et al. 2018)

$$J_{\text{ic}}(\nu) \approx \frac{c\sigma_T U_*}{8\pi\nu_*} \sqrt{\frac{\Gamma\nu(1+\mu)}{\nu_*}} N \left[\sqrt{\frac{\nu}{\Gamma\nu_*(1+\mu)}} \right] \quad (5)$$

Here, ν_* and U_* are the frequency and energy density of the external photon field, Γ is the bulk Lorentz factor of the jet and μ is the cosine of the jet viewing angle measured in the proper frame of the AGN. In the observer's frame, the total flux due to these radiative processes can be obtained after considering the relativistic and cosmological effects (Begelman et al. 1984; Dermer 1995)

$$F_{\text{obs}}(\nu_{\text{obs}}) = \frac{\delta_D^3(1+z)}{d_L^2} V J_{\text{syn/ic}} \left(\frac{1+z}{\delta_D} \nu_{\text{obs}} \right) \quad (6)$$

Here, $V = 4/3\pi R_{\text{knot}}^3$ is the volume of the emission region, z is the source redshift, d_L is the luminosity distance and $\delta_D = 1/[\Gamma(1-\beta\mu)]$ is the jet Doppler factor.

3.1 Source Parameters

The observed spectrum due to IC/CMB model is mainly governed by 8 source parameters with 4 of them K , p , q and γ_b governing the electron distribution, and the rest are the size of the emission region R_{knot} , magnetic field B , jet Lorentz factor Γ and the jet viewing angle θ . Besides these, the parameters γ_{\min} and γ_{\max} do not govern the source fluxes rather decide the low and high energy end of radiation spectrum (see section 4). Limited amount of information available in radio, optical and X-ray bands do not let us to draw stringent constraints on these parameters. However, modest constraints can be imposed by assuming equipartition between the magnetic field and particle energy densities (equation 3) and the emission region size of kilo-parsec scale order which is consistent with the typical radio contours of the knots.

The synchrotron flux at radio/optical in combination with equation 3 can effectively constrain B and K while, the spectral indices can be used to identify p and q . The synchrotron spectral peak frequency can be expressed in terms of the source parameters as

$$\nu_{p,\text{syn}} = \frac{\delta_D}{1+z} \gamma_b^2 \frac{eB}{2\pi m_e c} \quad (7)$$

For a given δ_D , γ_b can be estimated from the approximate peak frequency. With these constraints we will be left with the parameters Γ and θ which can be fine-tuned to reproduce the X-ray flux due to IC/CMB process. The approximate analytical expressions for the synchrotron and IC/CMB fluxes are used only to estimate the source parameters. The final model spectrum is produced numerically using exact functional form of the single particle emissivities and compared with the observed fluxes.

An upper limit on the angle of the jet to the line of sight (θ) can be drawn from the apparent superluminal motion obtained through Very Long Baseline Interferometry (VLBI) observations. Breiding et al. (2023) estimate the upper limits on θ for 3C 111, 3C 120, PKS 1045-188 and 3C 454.3 to be 13.5° , 12.6° , 10.5° and 4.5° respectively. An upper limit of 13° is estimated for jet inclination angle of PKS B0106+013 (Kharb et al. 2012). Harris et al. (2017) using the apparent superluminal proper motions of pc-scale jet estimate that the kpc-scale jet of PKS 1354+195 is aligned at $\theta \leq 12^\circ$. Dulwich et al. (2009) calculate the viewing angle of 3C 346 to be $\theta = 14 \pm 8^\circ$. The apparent velocity measurements of 3C 15 is not available. However, Leahy et al. (1997) found its jet/counter-jet flux density ratio and puts a constraint of $\theta \approx 45^\circ - 50^\circ$ for $\beta \geq 0.9$. But, in order to explain the X-ray emission through IC/CMB model, the jet inclination should be less than the angle constraint drawn from jet/counter-jet ratio. Therefore in this work, θ is chosen such that the model curve fits with the observations. The apparent velocity or jet/counter-jet measurements for sources 3C 17 and PKS 2101-490 are not available. Therefore, viewing angle for these sources are chosen such that the IC/CMB model curve can fit with the radio-optical-X-ray observations of the knots. The sizes of individual knots are constrained using radio data and the value of R_{size} is listed in table 2.

4 RESULTS AND DISCUSSION

We apply the IC/CMB model to reproduce the X-ray flux of 18 knots/jet components from the sources which are not ruled out by initial *Fermi* observations (Table 1). As mentioned earlier, the initial guess parameters are derived from approximate analytical expressions for the emissivity functions and are then fine tuned to reproduce the radio-optical-X-ray fluxes using exact numerical solution. The best fit model parameters (chi-by-eye) for these knots are given in Table 2 with their corresponding SEDs shown in Figure 1 and 2.

The parameters γ_{min} and γ_{max} cannot be constrained from the available information and we have fixed these quantities at 50 and $10^3 \times \gamma_b$ ($\sim 10^8 - 10^9$) respectively for all the SEDs. The Compton up-scattered photon energy scales as γ^2 and hence this choice of γ_{max} assures the Compton spectral component extend up to sixth order from the spectral peak. The gyro-radius of the electron corresponding to γ_{max}

is $\sim 10^{-2} - 10^{-1}$ pc, which is much less than the assumed size of the knot. Therefore, this ensures that such high energy electrons can still be confined within the emission region. The equipartition magnetic field depends on γ_{min} , since the particle energy density is largely decided by the electrons at this energy. However, we noted that moderate variation in γ_{min} (within the same order) do not alter our conclusions significantly.

In order to predict the VHE flux from these knots/jets, we extended the IC/CMB model spectrum to VHE energies. The VHE photons produced from distant sources undergo significant attenuation through pair production process with the extragalactic background light (EBL). To account for this, we have considered the EBL spectrum provided by Franceschini & Rodighiero (2017) and the attenuated VHE spectrum is compared with the 50 hour sensitivity curve of CTAO obtained from CTAO webpage². In Fig 1 and 2, the blue solid line is the VHE spectrum after accounting for the EBL induced attenuation. The red, green and magenta solid line are the 50 hour CTAO differential sensitivities of Omega, Alpha (both Northern array) and Omega configuration (Southern array) respectively. The *Fermi* gamma-ray upper limits/detections are shown as green color inverted triangles/solid circles. Out of all the knots studied, we find the knots of 3C 111 (K 30), 3C 120 (K 4) and a section of 3C 120 jet (S 2) fall within the detection threshold of CTAO. The SED corresponding to these knots/jet is shown in Fig. 1 along with the CTAO sensitivity curve. The knots whose VHE model flux fall below the CTAO sensitivity curve are shown in Fig. 2. Moreover, both 3C 120 and 3C 111 can be detected from the Northern site of the Cherenkov Telescope Array (CTA) at reasonable zenith angles.

Among the two sources predicted as a CTAO VHE candidate under IC/CMB model, 3C 111 belongs to FR II morphology (Fanaroff & Riley 1974) located at $z=0.049$. The radio observation suggests a 100 kilo-parsec long jet and *Chandra* was able to resolve nearly 10 knots with at least eight which are prominent in X-rays (Clautice et al. 2016). Among them, the knots K 22, K 30 and K 61 indicate a hard X-ray spectrum suggesting an inverse Compton origin of the X-ray emission. Whereas, the knots K 9, K 14, K 38, K 45, K 51, K 97 and K 107 has steeper X-ray spectrum supporting a synchrotron origin (Zhang et al. 2018). Hence, for the present work we have considered only the three X-ray knots K 30, K 61 and K 22, with K 30 being the brightest among them. Modelling the X-ray emission as IC/CMB mechanism predicts significant VHE flux for the knot K 30 which can be examined by future CTAO observations. The predicted VHE flux of K 61 and K 22 fall below the CTAO sensitivity though the X-ray flux of K 61 is comparable with K 30. We anticipate the reason for this being the steep X-ray spectrum of K 61 as compared to K 30.

Recently, (Breiding et al. 2023) ruled out the IC/CMB interpretation of the X-ray emission for 3C 111 considering the knot K 61 through the updated *Fermi* upper limits (these upper limits are shown as blue inverted triangles in Fig. 1 and 2). However, the steep X-ray index of the knot K 61 is not consistent with the model spectrum and this can cause ambiguity (See Fig. A6 in (Breiding et al. 2023)). On the other

² <https://www.cta-observatory.org/science/cta-performance/>

hand, the X-ray spectrum of K30 is hard and can provide better constraints. Comparing the predicted gamma ray flux of this knot with the updated *Fermi* upper limits again disfavours the IC/CMB interpretation. Nevertheless, studying this source at VHE will be an additional confirmation to this conjecture or may provide stronger constraints on the emission model if detected.

The second source predicted as a VHE candidate for CTAO under IC/CMB model is 3C 120 located at $z=0.033$ which is a broad line radio galaxy initially classified as Seyfert I (Sahakyan et al. 2015). The radio morphology of the source is similar to FR I class with radio structures extending up to 100 kpc and superluminal components identified with VLBI studies (Walker et al. 2001, 1987). The X-ray jet consists of four bright knots K4, K7, K25 and K80 and two sections of the jet S2 and S3 bright in X-rays (Harris et al. 1999). The X-ray spectrum for the knot K7 and the jet component S3 is steep supporting a synchrotron origin while K4 and S2 suggests IC/CMB origin due to hard X-ray spectrum. The knots K25 and K80 are not well resolved in optical waveband (Harris et al. 2004). Hence, in this work we have considered only the knot K4 and the jet component S2, and modelled their X-ray emission through IC/CMB process. Extrapolating this emission model to VHE suggests, the gamma-ray flux from these regions fall within the 50-hour sensitivity of CTAO. In Fig. 1, we show the model spectrum corresponding to synchrotron and IC/CMB emission processes along with the observed radio–optical–X-ray fluxes. The CTAO sensitivity curve is shown in red solid line while the *Fermi* gamma-ray upper limits/detections are shown as green color inverted triangles/solid circles. Though the model curve falls within this *Fermi* upper limits, recent upper limits (blue inverted triangles in Fig.1) derived from 12 years of observation again disfavours the IC/CMB model for this source also (Breiding et al. 2023).

The analytical approximation for the inverse Compton emissivity (equation (5)) is arrived considering the scattering process to happen in Thomson regime. However, at VHE energy the scattering may be inelastic and better described by the Klein-Nishina cross section. In order to investigate this, we draw limits on the target photon energy beyond which the scattering process deviates from the Thomson condition (Ghisellini & Tavecchio 2009). This happens when the target photon energy measured in the electron rest frame exceeds (or equal to) the rest mass energy (Blumenthal & Gould 1970). Using this condition along with the scattered photon energy estimated under Thomson regime, one can arrive the condition on target photon frequency as (Ghisellini & Tavecchio 2009; Sahayanathan & Godambe 2012)

$$\begin{aligned} \nu^* &\lesssim \frac{1}{\nu(1+z)} \left(\frac{\delta_D}{\Gamma} \right) \left(\frac{mc^2}{h} \right)^2 \\ &\lesssim 10^{14} \left(\frac{\delta_D}{\Gamma} \right) \left(\frac{\nu}{10^{26}} \right)^{-1} \text{ Hz} \end{aligned} \quad (8)$$

where, ν^* is the frequency of target photon in AGN frame, ν is the scattered photon (VHE) frequency in observer frame and $\delta_D/\Gamma \approx 1.5$ (for $\Gamma = 4.0$ and $\theta = 9^\circ$ corresponding to the knot K30 of 3C111). For IC/CMB process the target photon frequency is $\approx 1.6 \times 10^{11}$ Hz and the scattering falls within the Thomson regime. Nevertheless, in the numerical code used to reproduce the model spectrum we have consid-

ered the exact Klein-Nishina cross section for the IC scattering (Dermer & Schlickeiser 1993).

The jet components (or knots) considered in this work are located at kilo-parsec scale distances from the AGN core. For instance, the jet components that fall within the detection threshold of CTAO, K4 and S2 of 3C 120 are at distances larger than 2.5 kpc from their core (Harris et al. 1999). And the knot K30 of 3C 111 is approximately at a distance of 60 kpc from the core (Clautice et al. 2016). At this large scale distances, the dominant photon field is Cosmic Microwave Background Radiation (CMBR) compared to other photon fields associated with galaxy. Additionally, the relativistic boosting increases the energy density of the CMB in the jet frame by Γ^2 while, other external photon field like starlight, thermal infrared radiation from the dusty torus and emission from the accretion disk fall behind the relativistic motion of the emission region and hence, their energy density will be reduced by $\approx \Gamma^2$ (Begelman et al. 1984). Hardcastle & Croston (2011) has modelled the TeV γ -ray emission from M87 and Cen A considering inverse Compton scattering of various photon fields by the high-energy electrons responsible for the synchrotron X-rays on kiloparsec scale. However, for this study they have considered only the inner jet region which fall within a kpc from core and the contribution of photon fields other than CMB are also substantial.

In this work, we attempt to study the AGN with misaligned jets which are the probable VHE candidates for CTAO. Such misaligned AGN jets have already been studied at VHE and the first significant detection was the FR I source M87 located at a distance 16 Mpc ($z = 0.0043$) (Aharonian et al. 2006). Observations of this source from 2003 till 2006 by H.E.S.S witness the flux variability in timescale of few days. Constraints on the emission region size drawn from this variability timescale suggests the VHE emission to be arising very close to the central engine. The plausible locations are the bright inner most knot HST-1 or the nucleus of M87. Different emission models have been proposed favouring either of these regions albeit a consensus was never arrived (Rieger & Aharonian 2008; Lenain et al. 2008; Levinson & Rieger 2011; Hardcastle & Croston 2011; Fraija et al. 2012; Rieger 2012).

The other misaligned AGN which are detected in VHE are Cen A (Aharonian et al. 2009), NGC 1275 (Aleksić et al. 2012), 3C 264 (Holder 2011), PKS 0625-354 (HESS Collaboration et al. 2018) and IC 310 (Aleksić et al. 2010). An important challenge often encountered while explaining the VHE emission from these sources is the necessity of substantial Doppler boosting. In case of blazars, the jet is aligned close to the line of sight and hence the emission is significantly Doppler boosted. This allow the gamma ray emission to overcome the pair production losses since the rest frame photon energy is less than the observed energy (Dondi & Ghisellini 1995). In case of misaligned AGN, the Doppler boosting will be minimal due to large viewing angle of the jet. This introduces strong constraints on the choice of the bulk Lorentz factor of the jet and the viewing angle (Singal 2016). However, the viewing angle inferred from studying the broadband spectral energy distribution of the source often conflicts with the ones obtained through radio morphological studies (Reynoso et al. 2011; Fujita & Nagai 2017).

The low energy tail of the electron distribution upscatter-

ing the CMB photons to X-ray energies are also responsible for the radio emission through synchrotron process. This predicts the knots observed at these energy bands to be co-spatial. However, the observed offset between X-ray and radio centroids of the knots from the large scale jets contradict this co-spatiality (Reddy et al. 2021). The relatively longer cooling time of low energy electrons also suggest the X-ray emission to be persistent downstream in the jet along with radio. However, in many cases, X-ray emission is localized and do not show continuity similar to radio maps (Harris et al. 2006). These observational features advocate against the IC/CMB interpretation of the X-ray emission.

Another line of evidence challenging IC/CMB is the detection of X-ray counter jet in Pictor A (Hardcastle et al. 2016). The jet counter-jet ratio for this source suggests the jet viewing angle $\theta < 45^\circ$ and the jet velocity $v \leq 0.5c$. The IC/CMB models for the X-ray emission; on the other hand, demands larger jet velocity to boost the CMB photons significantly in the frame of the emission region. Accordingly, smaller viewing angles are also assumed. Similarly, the high degree of X-ray polarisation witnessed in certain knots (Cara et al. 2013), the knot flux variability (Hardcastle et al. 2016) and the deficit of correlation between the ratio of X-ray to radio jet luminosity with the source redshift (Snios et al. 2021) poses strong challenges to the IC/CMB interpretation of the X-ray emission. Observation of the sources 3C 111 and 3C 120 in VHE can further verify this emission model and in addition, provide clues regarding the high energy emission process.

5 SUMMARY

The high energy emission from the knots of kpc scale AGN jet is often interpreted as the inverse Compton up-scattering of Cosmic microwave background radiation by relativistic particles in the jet (IC/CMB). However, the gamma-ray upper limits derived from the long term observation of these sources by *Fermi* disfavours this interpretation. In this work, we perform a detailed multiwavelength modelling of the knots of the AGN jets which are detected in X-rays using synchrotron and IC/CMB processes. The source parameters deciding the broadband spectral energy distribution are estimated using approximate analytical expression for the emissivity functions. The emission model is extrapolated to VHE energy and then compared with the CTAO sensitivity. We find the VHE model flux of certain knots/jet components of two sources, 3C 111 and 3C 120, fall well above the CTAO sensitivity. However, the recently updated *Fermi* upper limits again disfavours IC/CMB interpretation for the high energy emission from these sources. Therefore any sources in our study, if detected in VHE, would probably favour the second population interpretation for the high energy emission rather than IC/CMB.

ACKNOWLEDGEMENTS

A.A.R acknowledge Dr.Gulab Dewangan and Inter-University Centre for Astronomy and Astrophysics(IUCAA), Pune, India for the support and research facilities. A.A.R is thankful to the financial support provided by University Grants Commission (UGC), Govt. of India. A.A.R is also grateful to the unknown reviewer for the valuable comments.

DATA AVAILABILITY

The data and the codes used in this work will be shared on the reasonable request to the corresponding author Amal A. Rahman (email:amalar.amal@gmail.com)

REFERENCES

- Aharonian F., et al., 2006, *Science*, **314**, 1424
 Aharonian F., et al., 2009, *ApJ*, **695**, L40
 Aleksić J., et al., 2010, *ApJ*, **723**, L207
 Aleksić J., et al., 2012, *A&A*, **539**, L2
 Atoyan A., Dermer C. D., 2004, *ApJ*, **613**, 151
 Begelman M. C., Blandford R. D., Rees M. J., 1984, *Reviews of Modern Physics*, **56**, 255
 Blumenthal G. R., Gould R. J., 1970, *Reviews of Modern Physics*, **42**, 237
 Breiding P., 2018, PhD thesis, University of Maryland, Baltimore County
 Breiding P., Meyer E. T., Georganopoulos M., Keenan M. E., DeNigris N. S., Hewitt J., 2017, *ApJ*, **849**, 95
 Breiding P., Meyer E. T., Georganopoulos M., Reddy K., Kollmann K. E., Roychowdhury A., 2023, *MNRAS*, **518**, 3222
 Burbidge G. R., 1959, *ApJ*, **129**, 849
 Cara M., et al., 2013, *ApJ*, **773**, 186
 Chartas G., et al., 2000, *ApJ*, **542**, 655
 Clautice D., et al., 2016, *ApJ*, **826**, 109
 Dermer C. D., 1995, *ApJ*, **446**, L63
 Dermer C. D., Menon G., 2009, High Energy Radiation from Black Holes: Gamma Rays, Cosmic Rays, and Neutrinos
 Dermer C. D., Schlickeiser R., 1993, *ApJ*, **416**, 458
 Dondi L., Ghisellini G., 1995, *MNRAS*, **273**, 583
 Dulwich F., Worrall D. M., Birkinshaw M., Padgett C. A., Perlman E. S., 2007, *MNRAS*, **374**, 1216
 Dulwich F., Worrall D. M., Birkinshaw M., Padgett C. A., Perlman E. S., 2009, *MNRAS*, **398**, 1207
 Dyrda M., Wierzcholska A., Moderski R., Ostrowski M., Stawarz L., 2015, in 34th International Cosmic Ray Conference (ICRC2015). p. 801 ([arXiv:1509.06851](https://arxiv.org/abs/1509.06851)), doi:10.22323/1.236.0801
 Fanaroff B. L., Riley J. M., 1974, *MNRAS*, **167**, 31P
 Fraija N., González M. M., Pérez M., 2012, in Gamma-Ray Bursts 2012 Conference (GRB 2012). p. 131 ([arXiv:1212.4424](https://arxiv.org/abs/1212.4424)), doi:10.22323/1.152.0131
 Franceschini A., Rodighiero G., 2017, *A&A*, **603**, A34
 Fujita Y., Nagai H., 2017, *MNRAS*, **465**, L94
 Georganopoulos M., Perlman E. S., Kazanas D., McEney J., 2006, *ApJ*, **653**, L5
 Ghisellini G., Tavecchio F., 2009, *MNRAS*, **397**, 985
 Godfrey L. E. H., et al., 2012, *ApJ*, **755**, 174
 HESS Collaboration et al., 2018, *MNRAS*, **476**, 4187
 Hardcastle M. J., Croston J. H., 2011, *MNRAS*, **415**, 133
 Hardcastle M. J., Birkinshaw M., Worrall D. M., 2001, *MNRAS*, **326**, 1499
 Hardcastle M. J., et al., 2016, *MNRAS*, **455**, 3526
 Harris D. E., Krawczynski H., 2002, *ApJ*, **565**, 244
 Harris D. E., Krawczynski H., 2006, *ARA&A*, **44**, 463
 Harris D. E., Hjorth J., Sadun A. C., Silverman J. D., Vestergaard M., 1999, *ApJ*, **518**, 213
 Harris D. E., Mossman A. E., Walker R. C., 2004, *ApJ*, **615**, 161
 Harris D. E., Cheung C. C., Biretta J. A., Sparks W. B., Junor W., Perlman E. S., Wilson A. S., 2006, *ApJ*, **640**, 211
 Harris D. E., et al., 2017, *ApJ*, **846**, 119
 Holder J., 2011, in International Cosmic Ray Conference. p. 137 ([arXiv:1111.1225](https://arxiv.org/abs/1111.1225)), doi:10.7529/ICRC2011/V12/H11
 Kataoka J., Stawarz L., 2005, *ApJ*, **622**, 797

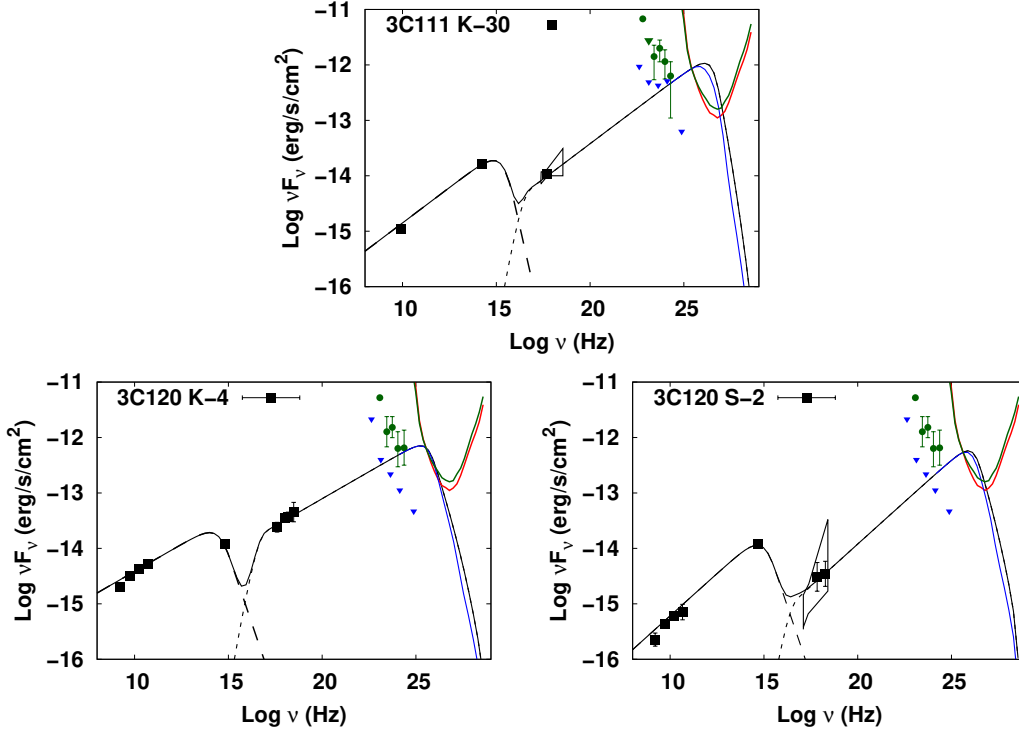


Figure 1. Large scale knots falling within the detection threshold of CTAO. Dashed line and dash-dotted line are the synchrotron and IC/CMB model curves respectively. The black solid line represents the synchrotron+IC/CMB curve. Solid squares are the multiwavelength observational data of the knots. Red solid line and green solid line is the differential sensitivities of CTAO-Northern array Omega(50 hour) and Alpha configuration respectively. Blue solid line is the IC/CMB model curve corrected for EBL absorption. Inverted triangles (green) and solid circles (green) are the *Fermi* upper limit values and *Fermi* observations (Xue et al. 2017). Inverted triangles (blue) are the updated *Fermi* upper limit values (Breiding et al. 2023). *Fermi*-LAT points (solid circles) correspond to the total observed emission, while the upper limits (inverted triangles) were derived specifically for the emission from the extended jet.

Source	<i>Knot</i>	p	q	$R_{knot}(kpc)$	Γ	θ	$\gamma_b(10^6)$	$B(10^{-6}G)$
3C 15	K C	2.15	3.60	3.0	6.0	9	0.27	4.10
3C 17	KS3.7	2.30	3.80	5.9	4.0	10	0.39	5.32
3C 17	KS11.3	2.30	4.3	4.5	6.0	10	0.29	7.78
3C 111	K 22	2.25	3.8	4.0	8.0	9	0.44	1.53
3C 111	K 30	2.49	6.0	5.5	4.0	9	5.92	2.34
3C 111	K 61	2.60	4.1	4.4	6.0	9	0.52	3.45
3C 120	K 4	2.61	5.0	3.0	8.0	8	1.68	3.63
3C 120	KS 2	2.40	6.0	1.0	7.0	8	4.28	2.32
PKS 1354+195	KS4.0	2.20	3.5	9.0	7.5	11	0.55	6.56
PKS 1354+195	KS5.3	2.40	3.7	3.8	8.0	11	0.13	11.98
3C 346	K C	2.40	4.2	1.8	6.0	9	0.57	15.77
3C 454.3	K A	2.60	4.0	4.0	4.7	4.5	0.13	14.51
3C 454.3	K B	2.60	4.5	2.2	4.7	4.5	0.15	35.50
PKS 2101-490	KK6	2.40	4.3	4.3	6.0	10	0.29	14.63
PKS B0106+013	Knot 1	2.20	4.1	2.0	3.0	13	0.12	44.73
PKS B0106+013	Knot 2	2.01	4.40	3.0	4.0	13	0.10	60.52
PKS B0106+013	Knot 3	2.05	4.40	1.0	2.0	13	0.02	255.75
PKS 1045-188	K C	2.20	4.30	5.0	9.0	8	0.16	6.69

Table 2. Fit parameters of radio-optical-X-ray spectrum. p and q are the power-law indices of particle distribution; R_{knot} is the radius of the knot; Γ , θ and γ_b are the bulk Lorentz factor, viewing angle of the jet and break energy of particle spectrum respectively. B is the magnetic field in micro-Gauss unit.

Kataoka J., Leahy J. P., Edwards P. G., Kino M., Takahara F., Serino Y., Kawai N., Martel A. R., 2003, *A&A*, **410**, 833
 Kharb P., Lister M. L., Marshall H. L., Hogan B. S., 2012, *ApJ*, **748**, 81
 Leahy J. P., Black A. R. S., Dennett-Thorpe J., Hardcastle M. J., Komissarov S., Perley R. A., Riley J. M., Scheuer P. A. G.,

1997, *MNRAS*, **291**, 20
 Lenain J. P., Boisson C., Sol H., Katarzyński K., 2008, *A&A*, **478**, 111
 Levinson A., Rieger F., 2011, *ApJ*, **730**, 123
 Liu W.-P., Chen Y. J., Wang C.-C., 2015, *ApJ*, **806**, 188
 Lucchini M., Tavecchio F., Ghisellini G., 2017, *MNRAS*, **466**, 4299

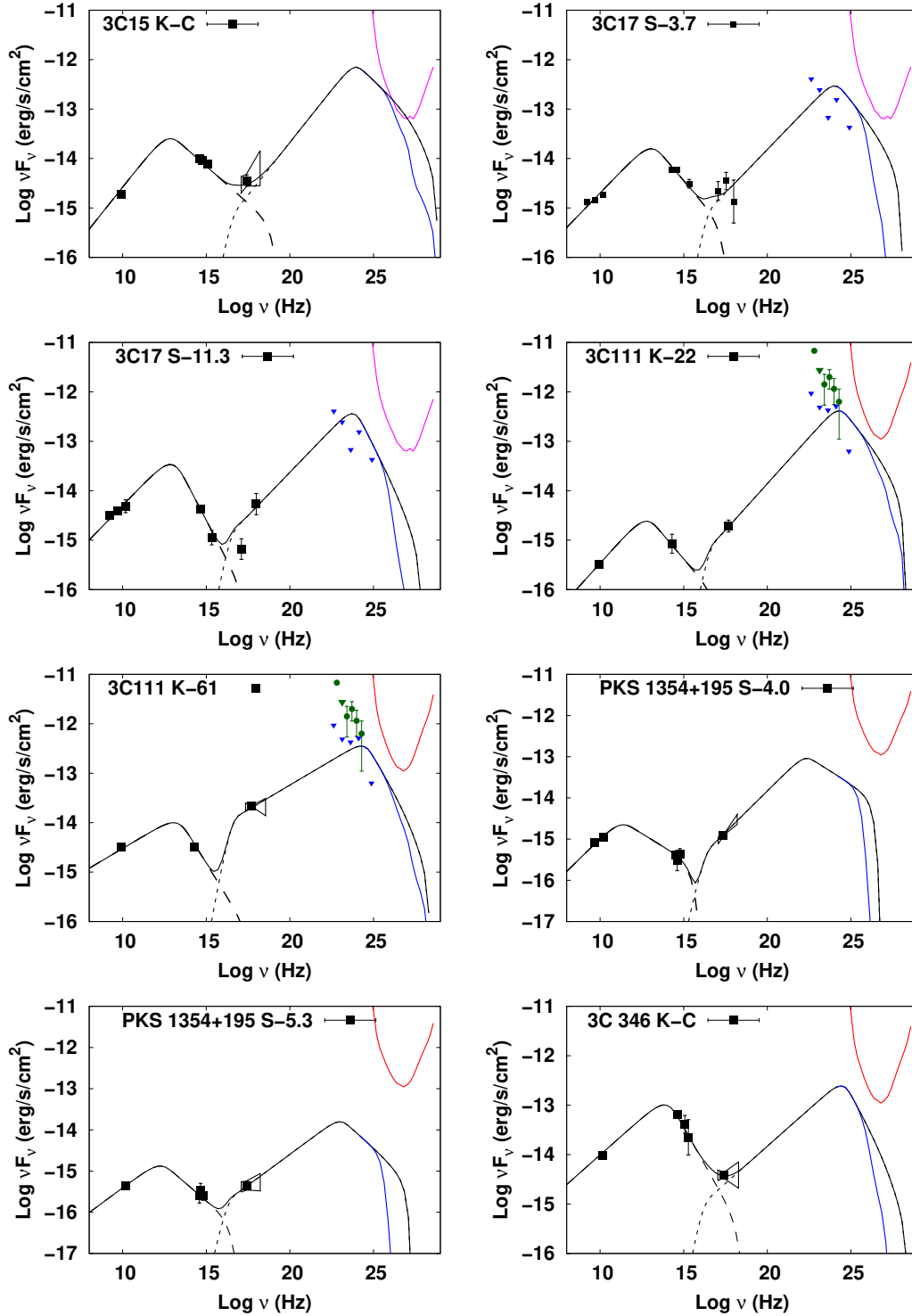


Figure 2. Large scale knots that do not fall within the detection threshold of CTAO. Dashed line and densely-dashed line are the synchrotron and IC/CMB model curves respectively. The black solid line represents the synchrotron+IC/CMB curve. Dotted lines represent the SSC model curve. Solid squares are the multiwavelength observational data of the knots. Blue solid line is the IC/CMB model curve corrected for EBL absorption. Red solid line and green solid line is the differential sensitivities of CTAO-Northern array Omega(50 hour) and Alpha configuration respectively. The magenta solid curve correspond to differential sensitivities of CTAO-Southern array Omega configuration (50 hour). Inverted triangles(green) and solid circles(green) are the *Fermi* upper limit values and *Fermi* observations for 3C111 and 3C 454.3 (Xue et al. 2017; Zhang et al. 2015). Blue inverted triangles/solid circles are the recent *Fermi* upper limit values/observations (Breiding et al. 2023). *Fermi*-LAT points(solid circles) correspond to the total observed emission, while the upper limits(inverted triangles) were derived specifically for the emission from the extended jet.

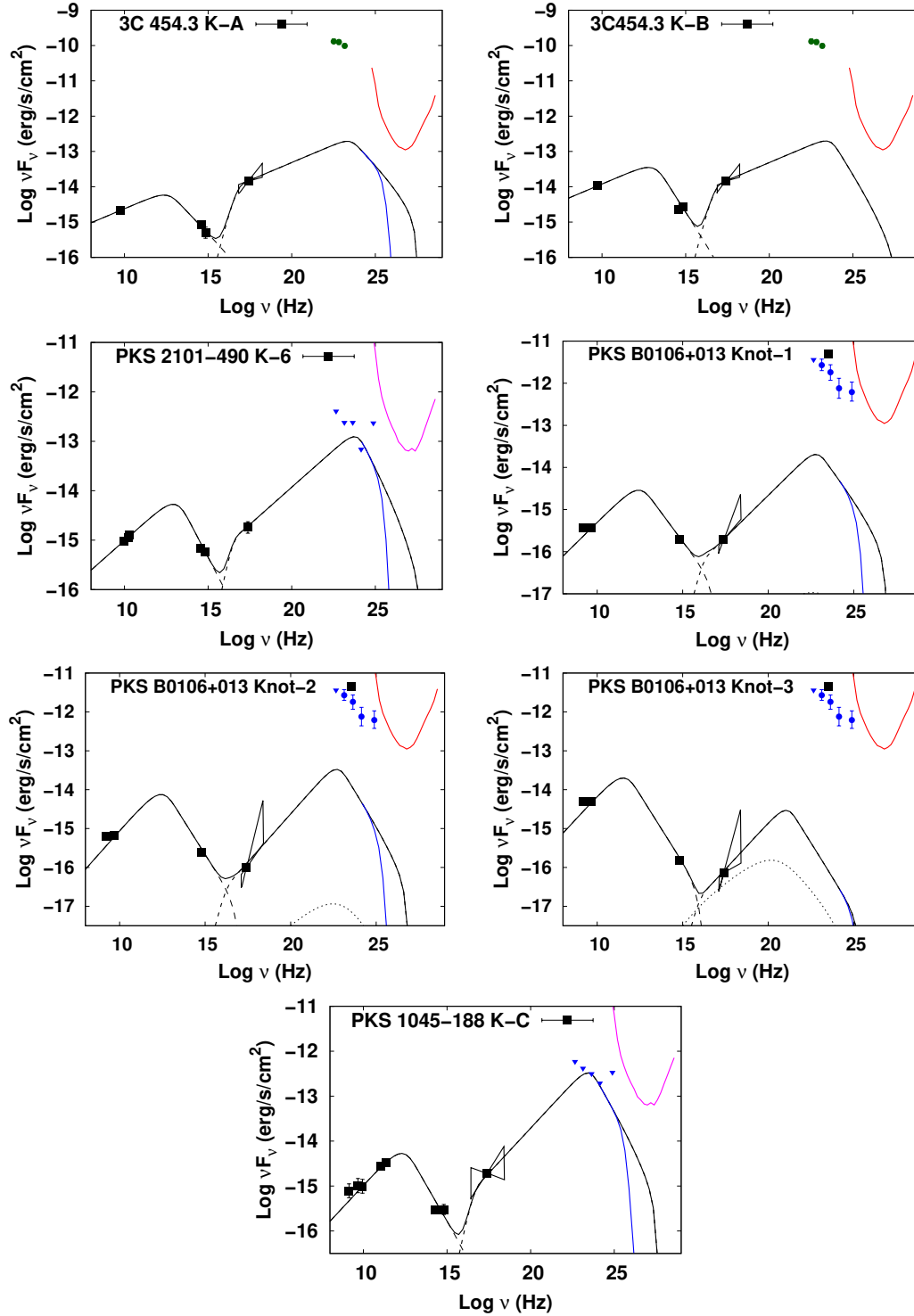


Figure 2 – continued

Massaro F., Harris D. E., Chiaberge M., Grandi P., Macchetto F. D., Baum S. A., O’Dea C. P., Capetti A., 2009, *ApJ*, **696**, 980
 Massaro F., Harris D. E., Cheung C. C., 2011, *ApJS*, **197**, 24
 Massaro F., et al., 2018, *ApJS*, **234**, 7
 Meyer E. T., Georganopoulos M., 2014, *ApJ*, **780**, L27
 Meyer E. T., Georganopoulos M., Sparks W. B., Godfrey L., Lovell J. E. J., Perlman E., 2015, *ApJ*, **805**, 154

Meyer E. T., Iyer A. R., Reddy K., Georganopoulos M., Breiding P., Keenan M., 2019, *ApJ*, **883**, L2
 Meyer E., Roychowdhury A., Georganopoulos M., 2021, in American Astronomical Society Meeting Abstracts. p. 238.05
 Perlman E. S., et al., 2011, *ApJ*, **739**, 65
 Rahman A. A., Sahayanathan S., Subha P. A., 2022, *MNRAS*, **515**, 1410
 Reddy K., Georganopoulos M., Meyer E. T., 2021, *ApJS*, **253**, 37

- Reynoso M. M., Medina M. C., Romero G. E., 2011, *A&A*, **531**, A30
- Rieger F. M., 2012, in Aharonian F. A., Hofmann W., Rieger F. M., eds, American Institute of Physics Conference Series Vol. 1505, High Energy Gamma-Ray Astronomy: 5th International Meeting on High Energy Gamma-Ray Astronomy. pp 80–87 ([arXiv:1210.6847](https://arxiv.org/abs/1210.6847)), doi:10.1063/1.4772223
- Rieger F. M., Aharonian F. A., 2008, *A&A*, **479**, L5
- Rulten C., 2022, *Galaxies*, **10**, 61
- Rybicki G. B., Lightman A. P., 1986, *Radiative Processes in Astrophysics*
- Sahakyan N., Zargaryan D., Baghmanyan V., 2015, *A&A*, **574**, A88
- Sahayanathan S., 2008, *MNRAS*, **388**, L49
- Sahayanathan S., Godambe S., 2012, *MNRAS*, **419**, 1660
- Sahayanathan S., Misra R., Kembhavi A. K., Kaul C. L., 2003, *ApJ*, **588**, L77
- Sahayanathan S., Sinha A., Misra R., 2018, *Research in Astronomy and Astrophysics*, **18**, 035
- Sambruna R. M., Urry C. M., Tavecchio F., Maraschi L., Scarpa R., Chartas G., Muxlow T., 2001, *ApJ*, **549**, L161
- Sambruna R. M., Maraschi L., Tavecchio F., Urry C. M., Cheung C. C., Chartas G., Scarpa R., Gambill J. K., 2002, *ApJ*, **571**, 206
- Schwartz D. A., et al., 2000, *ApJ*, **540**, 69
- Schwartz D. A., et al., 2006, *ApJ*, **647**, L107
- Siemiginowska A., Stawarz L., Cheung C. C., Harris D. E., Sikora M., Aldcroft T. L., Bechtold J., 2007, *ApJ*, **657**, 145
- Singal A. K., 2016, *ApJ*, **827**, 66
- Snios B., et al., 2021, *ApJ*, **914**, 130
- Stanley E. C., Kharb P., Lister M. L., Marshall H. L., O’Dea C., Baum S., 2015, *ApJ*, **807**, 48
- Stuardi C., et al., 2018, *ApJS*, **235**, 32
- Tavecchio F., 2021, *MNRAS*, **501**, 6199
- Tavecchio F., Maraschi L., Sambruna R. M., Urry C. M., 2000, *ApJ*, **544**, L23
- Tavecchio F., Maraschi L., Wolter A., Cheung C. C., Sambruna R. M., Urry C. M., 2007, *ApJ*, **662**, 900
- Wakely S. P., Horan D., 2008, in International Cosmic Ray Conference. pp 1341–1344
- Walker R. C., Benson J. M., Unwin S. C., 1987, *ApJ*, **316**, 546
- Walker R. C., Benson J. M., Unwin S. C., Lystrup M. B., Hunter T. R., Pilbratt G., Hardee P. E., 2001, *ApJ*, **556**, 756
- Wilson A. S., Young A. J., Shopbell P. L., 2001, *ApJ*, **547**, 740
- Worrall D. M., Birkinshaw M., 2005, *MNRAS*, **360**, 926
- Xue Z.-W., Zhang J., Cui W., Liang E.-W., Zhang S.-N., 2017, *Research in Astronomy and Astrophysics*, **17**, 090
- Zhang J., Bai J. M., Chen L., Liang E., 2010, *ApJ*, **710**, 1017
- Zhang J., Xue Z.-W., He J.-J., Liang E.-W., Zhang S.-N., 2015, *ApJ*, **807**, 51
- Zhang J., Du S.-s., Guo S.-C., Zhang H.-M., Chen L., Liang E.-W., Zhang S.-N., 2018, *ApJ*, **858**, 27

This paper has been typeset from a $\text{\TeX}/\text{\LaTeX}$ file prepared by the author.

